Supporting Information

Impact of High Charge-Collection Efficiencies and Dark Energy-Loss Processes on Transport, Recombination, and Photovoltaic Properties of Dye-Sensitized Solar Cells

Kai Zhu,* Song-Rim Jang, and Arthur J. Frank*

Chemical and Materials Science Center, National Renewable Energy Laboratory, Golden, Colorado 80401, USA

Experimental Method

Dye-sensitized TiO_2 solar cells (DSSCs) were fabricated as detailed elsewhere.[1] In brief, a thin compact layer of TiO_2 was deposited on a cleaned transparent conducting glass (TCO) plate (LOF TEC8 F-doped SnO_2 glass; Hartford Glass Company), using 0.2 M titanium diisopropoxide bis(acetylacetonate) in isopropanol by spray pyrolysis, followed by heating at 450 °C for 30 min. Mesoporous TiO_2 films were deposited via the screen-printing technique using a paste of 22 nm-sized TiO_2 nanoparticles on a TCO substrate and then sequentially sintered at 325 °C for 5 min, 375 °C for 5 min, 450 °C for 15 min, and 500 °C for 15 min. This film was then soaked in 0.02 M $TiCl_4$ solution at room temperature for 6 h and rinsed with distilled water. After sintering the films again at 500 °C in air for 30 min and cooling to 80 °C, they were immersed in a solution of acetonitrile and *tert*-butyl alcohol (1:1, v/v) containing 0.5 mM $[RuL_2(NCS)_2]$:2TBA (L = 2,2´-bipyridyl-4,4´-dicarboxylic acid; TBA = tetrabutylammonium; also known as the N719 dye) and 0.5 mM chenodeoxycholic acid (CDCA) for 15 h. The semitransparent counter electrode consisted of TCO covered with a Pt catalyst. Three types of electrolytes were used: (1) Electrolyte A was comprised of 1.0 M PMII (1-propyl-3-methylimidazolium iodide), 0.05 M LiI, 0.03 M I_2, 0.5 M *t*BP (4-*tert*-butylpyridine) and 0.1 M GNCS (guanidinium thiocyanate) in a solution of acetonitrile/valeronitrile (85:15, v/v); (2) Electrolyte B consisted of 0.6 M BMII (1-butyl-3-methylimidazolium iodide), 0.1 M LiI, 0.05 M I_2, 0.5 M *t*BP, and 0.1 M GNCS in a solution of acetonitle/valeronitrile (85:15, v/v); and (3) Electrolyte C was composed of 0.8 M HDMII (1-hexyl-2,3-dimethylimidazolium iodide) and 0.05 M I_2 in methoxypropionitrile. The porosity was 65% for all films. The average TiO_2 film thickness was about 10 μm as measured with a surface profiler (KLA Tencor Alpha-Step 500).

The photocarrier transport times at short circuit were measured by intensity modulated photocurrent spectroscopy (IMPS).[2,3] The photocarrier recombination times at open circuit were

* To whom correspondence should be addressed. E-mail: Kai.Zhu@nrel.gov; Arthur.Frank@nrel.gov.

measured by intensity modulated photovoltage spectroscopy (IMVS).[4,5] For these measurements, the DSSCs were probed with a small sinusoidally modulated beam of 680 nm light superimposed on a relatively large background (bias) illumination also at 680 nm. A semiconductor diode laser (680 nm) was used for this purpose. The probe and bias light entered the cell from the substrate side. Neutral density filters were used to vary the illumination intensity. The amplitude of the modulated photocurrent density was kept at 10% or lower compared to the steady-state photocurrent density. Electrochemical impedance spectroscopy (EIS) measurements were performed with a potentiostat/frequency analyzer (PARSTAT 2273) using a two-electrode configuration. The modulation frequencies range from 50 mHz to 100 kHz. The amplitude of the modulation voltage was 10 mV. Z-view 2.9c (Scribner Associates) was used to fit the EIS spectra to the equivalent circuit based on the transmission line model.[6] The total electron density in the TiO_2 films at open circuit was determined by the dark charge-extraction technique, similar to one reported previously.[7] Briefly, a constant voltage was applied across the cell in the dark using a potentiostat/frequency analyzer until a constant current was reached. The cell was then short circuited, and the resulting current transient was integrated to calculate the charge. The photoinduced electron density in the TiO_2 film at short circuit under illumination was determined by charge-extraction measurements.[8] The diode laser was driven with a pulsed voltage source (Stanford Research DS345), which allowed for a rapid on and off switching of the illumination. The actual photoinduced charge in the film was determined by numerically integrating the photocurrent decay using a digital oscilloscope (Tektronix DPO70404) after the steady-state light was switched off.

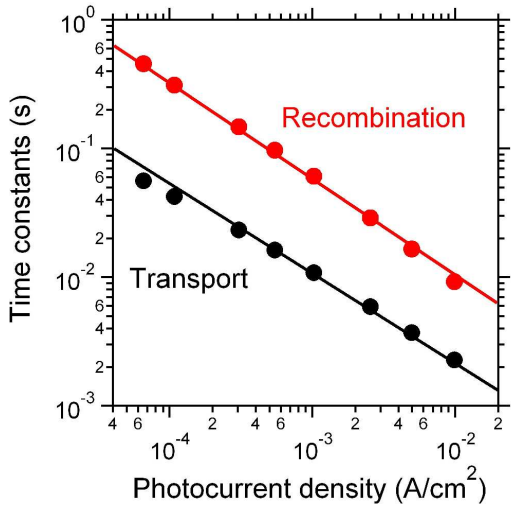

Figure S1. Dependence of transport (black circles) and recombination (red circles) time constants on the short-circuit photocurrent density for a DSSC with Electrolyte A.

Figure S1 shows the transport and recombination time constants at different short-circuit photocurrent densities J_{sc} for the same DSSC used in obtaining the *J–V* data in Figure 1. The transport and recombination time constants were measured under the same illumination condition (as indicated by J_{sc}) by IMPS at short circuit and IMVS at open circuit, respectively. Both the transport and recombination time constants exhibit a similar power-law dependence on the light intensity in concurrence with previous studies.[5,9,10] The power-law dependence of transport times on light intensity is generally attributed to electrons undergoing multiple trapping and detrapping during their transit through a film,[2,3,10-16] whereas the cause of nonlinear dependence of recombination times on light intensity is a subject of debate.[7,9,10,13,17,18]

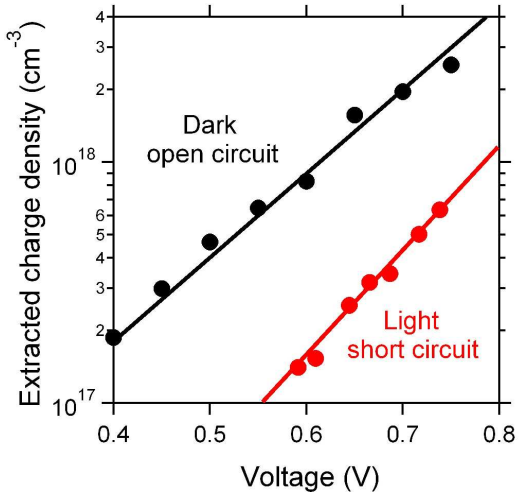

Figure S2. Plots of the extracted charge density as a function of voltage (or, quasi-Fermi level) at open circuit (black circles) and short circuit (red circles) for a DSSC with Electrolyte A.

Figure S2 shows the dependence of extracted charge density on the voltage (or quasi-Fermi level) for the same DSSC used in obtaining the *J–V* data in Figure 1. For the charge-extraction data obtained at open circuit in the dark (black circles), the voltages were applied to the cell before switching it to short circuit. The plot of charge density versus quasi-Fermi level is usually used to derive the trap distribution below the TiO_2 conduction bandedge.[19] Figure S2 also shows the plot for extracted charges measured at short circuit for cells under illumination (red circles). The voltages associated with this extracted charge, however, correspond to the open circuit values that were obtained for cells under the same illumination conditions used at short circuit in the charge-extraction measurements. The red curve is significantly lower than the black curve, implying that the charge density at short circuit is much less than that at open circuit. Thus, the difference in the voltage between the two plots reflects the difference in the quasi-Fermi levels of the cell between short circuit and open circuit at constant light intensity.[7]

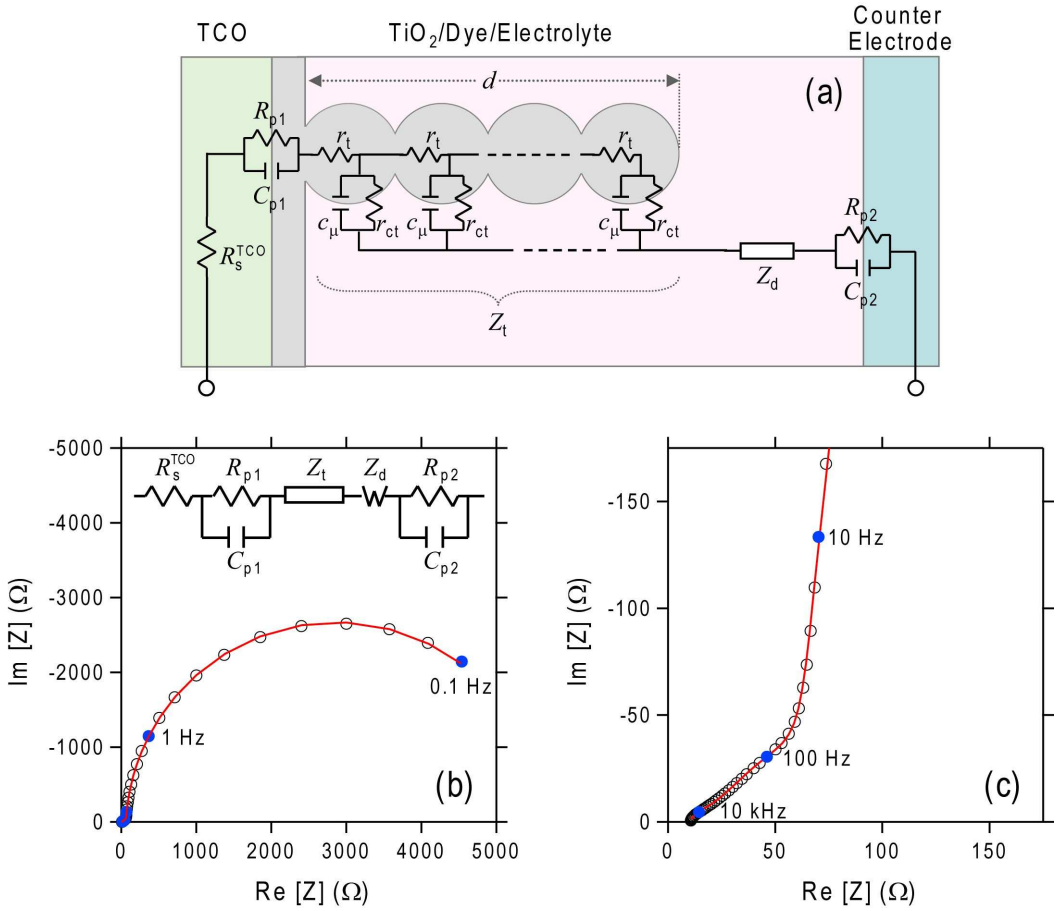

Figure S3. (a) Physical locations of equivalent circuit elements of a DSSC used for the EIS analysis, (b) typical Nyquist plot, and (c) high-frequency region of the Nyquist plot showing the impedance response of a DSSC with Electrolyte A under illumination measured at V_{oc} = 0.55 V. Inset shows the equivalent circuit model.

Figure S3a displays the physical location and interfaces of the equivalent circuit elements for a DSSC used for the EIS analysis. In the equivalent circuit model (inset of Figure S3b), R_s^{TCO} is the sheet resistance of TCOs, R_{p1} and C_{p1} are the respective charge-transfer resistances and interfacial capacitance at the TCO/TiO_2/electrolyte interface, Z_t is the transmission line element, Z_d is the Warburg impedance associated with ion diffusion in the electrolyte, and R_{p2} and C_{p2} are the respective charge-transfer resistances and interfacial capacitance at TCO/Pt/electrolyte interface. The transmission line element Z_t contains the distributed transport resistance r_t of electrons in the TiO_2 film, the recombination resistance r_{ct}, and the chemical capacitance c_μ at the TiO_2/electrolyte interface. For a TiO_2 film of thickness d, the corresponding total resistances and total capacitance are given by $R_t = r_t d$, $R_{ct} = r_{ct}/d$ and $C_\mu = c_\mu d$, respectively. Figure S3b,c shows the impedance spectrum for the same DSSC used in obtaining the J–V data in Figure 1 under illumination at 680 nm at open circuit. From these plots, three features of the

impedance response can be identified: (1) a large semicircle at low frequencies (from about 0.1 to 10 Hz), which corresponds to the charge-transfer process at TiO_2/redox electrolyte interface with a charge-transfer (recombination) resistance R_{ct}; (2) a linear region with 45° slope at medium frequencies (from about 100 to 10 kHz; Figure S3b), which is characteristic for the transmission line model[6] with the transport resistance R_t; and (3) a small semicircle at high frequencies (>10 kHz), which is associated with the charge-transfer process at the TCO/Pt/electrolyte interface and/or the TCO/TiO_2/electrolyte interface.

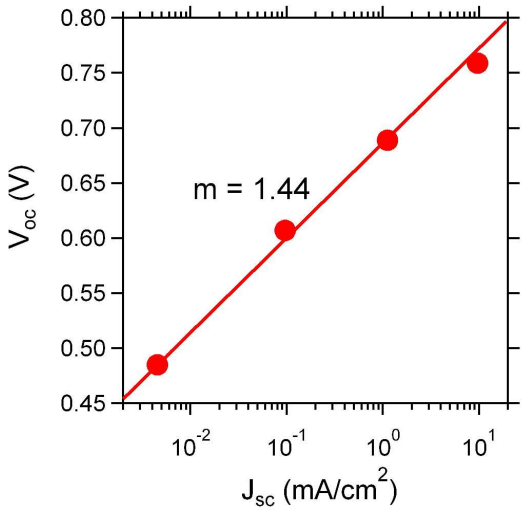

Figure S4. Dependence of open-circuit voltage V_{oc} on the short-circuit current density J_{sc} for the DSSC with Electrolyte A.

Figure S4 shows the dependence of the open-circuit voltage V_{oc} on J_{sc} for the DSSC used in obtaining the *J*–*V* data in Figure 1. The best fit (solid line) of the data to the exponential dependence of J_{sc} ($J_{sc} \propto \exp(qV_{oc}/mkT)$) yields the diode ideality factor $m = 1.44$.

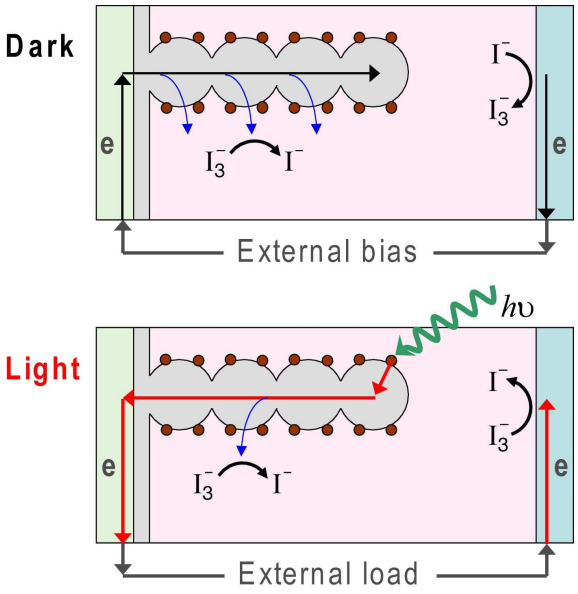

Figure S5. Schematics of the current flows in a DSSC in the dark and in the light.

Figure S5 shows schematics of the current flow in a DSSC in the dark and in the light. The net current density J_{net} that flows through the external circuit of a DSSC under illumination can be described by the superposition of the two opposing current flow: (1) the dark current density at forward applied bias J_F, flowing from the TCO substrate into the TiO_2 film; and (2) the light-generated photocurrent density J_L, flowing from the TiO_2 film into the TCO substrate.

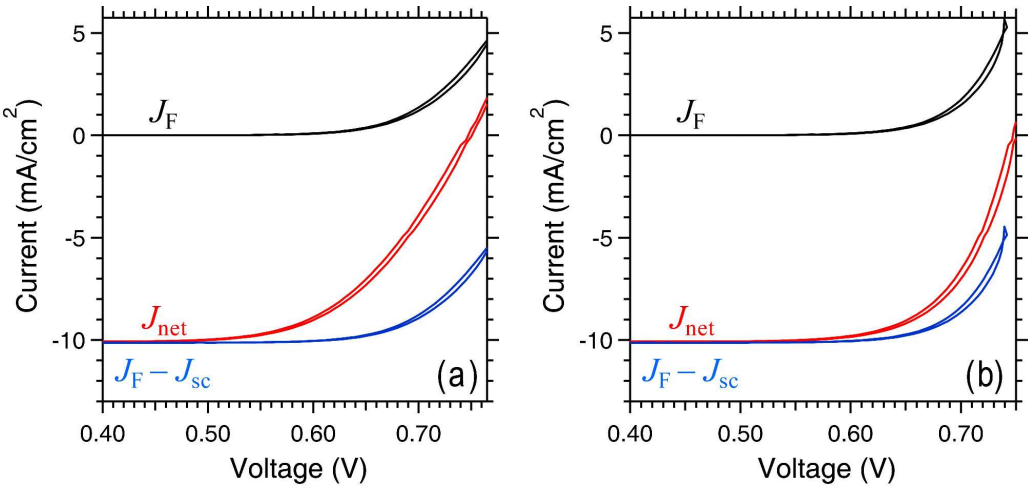

Figure S6. *J*–*V* characteristics of a DSSC with Electrolyte B, (a) before and (b) after correcting for ohmic losses: (1) J_F represents the current density at forward applied bias in the dark (denoted by the black J_F–*V* curve); (2) J_{net} represents the current density at applied biases when the cell is illuminated with 680 nm laser light (denoted by the red J_{net}–*V* curve); and (3) J_F–J_{sc} corresponds to J_F after being shifted by J_{sc} (denoted by the blue ($J_F - J_{sc}$)–*V* curve; eq 3).

Figure S6a compares the *J*–*V* characteristics of a DSSC with Electrolyte B in the dark and under laser illumination at 680 nm. The black J_F–*V* curve in Figure S6a shows the current density J_F in the dark at forward applied bias. The red J_{net}–*V* curve shows the current density J_{net} when the cell is illumined with 680 nm laser light. From the J_{net}–*V* curve, it can be seen that J_{sc} is 10.1 mA/cm^2, V_{oc} is 0.75 V, the maximum power point is at 0.58 V, and the fill factor FF is 0.72. The area between the J_{net}–*V* and ($J_F - J_{sc}$)–*V* curves represents the difference between the actual and ideal *J*–*V* characteristics of the DSSC. The photocurrent density loss increases significantly from 7% at the maximum power point to 64% at V_{oc}. The total power density loss, determined by integrating the area between J_{net}–*V* and ($J_F - J_{sc}$)–*V* curves, is about 17%. After correcting for ohmic losses in the same DSSC (Figure S6b), the photocurrent density loss was reduced from 7 to 4% at the maximum power point and from 64% to 29% at V_{oc}, and the total power density loss was reduced from 17% to 6%.

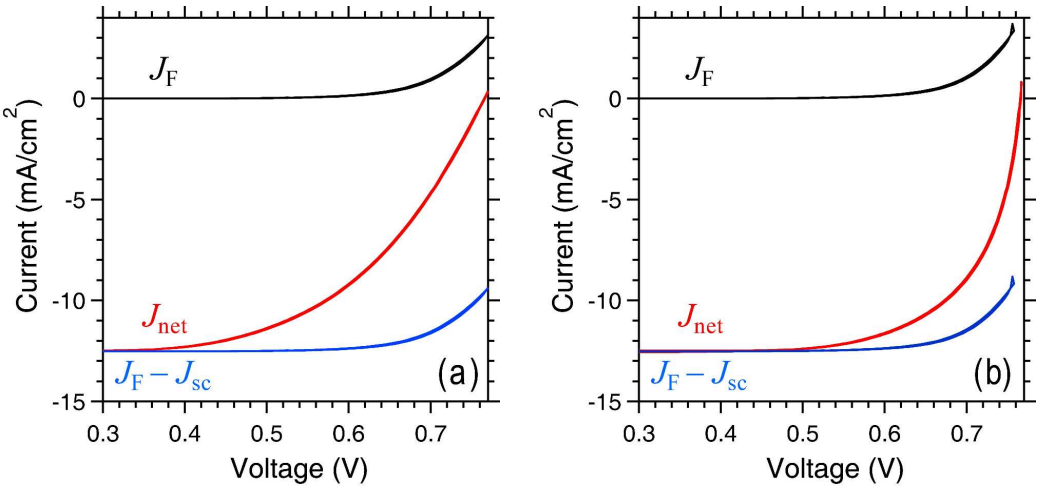

Figure S7. *J–V* characteristics of a DSSC with Electrolyte C, (a) before and (b) after correcting for ohmic losses: (1) J_F represents the current density at forward applied bias in the dark (denoted by the black J_F–V curve); (2) J_{net} represents the current density at applied biases when the cell is illuminated with 680 nm laser light (denoted by the red J_{net}–V curve); (3) J_F–J_{sc} corresponds to J_F after being shifted by J_{sc} (denoted by the blue ($J_F - J_{sc}$)–V curve; eq 3).

Figure S7a compares the *J–V* characteristics of a DSSC with Electrolyte C in the dark and under laser illumination at 680 nm. From the J_{net}–V curve, it can be seen that J_{sc} is 12.5 mA/cm^2, V_{oc} is 0.77 V, the maximum power point occurs is at 0.54 V, and FF is 0.61. The photocurrent density loss (the difference between the J_{net}–V and ($J_F - J_{sc}$)–V curves) increases from about 14% at the maximum power point to 76% at V_{oc}. The total power density loss, determined by integrating the area between J_{net}–V and ($J_F - J_{sc}$)–V curves, is about 40%. After correcting for ohmic losses in the same DSSC (Figure S7b), the photocurrent density loss was reduced from 14 to 10% at the maximum power point and from 76% to 67% at V_{oc}. Furthermore, after making the same correction the total power density loss was reduced from 40% to 26%.

REFERENCES

(1) Neale, N. R.; Kopidakis, N.; van de Lagemaat, J.; Grätzel, M.; Frank, A. J. Effect of a Coadsorbent on the Performance of Dye-Sensitized TiO_2 Solar Cells: Shielding Versus Band-Edge Movement. *J. Phys. Chem. B* **2005**, *109*, 23183-23189.

(2) Dloczik, L.; Ileperuma, O.; Lauermann, I.; Peter, L. M.; Ponomarev, E. A.; Redmond, G.; Shaw, N. J.; Uhlendorf, I. Dynamic Response of Dye-Sensitized Nanocrystalline Solar Cells: Characterization by Intensity-Modulated Photocurrent Spectroscopy. *J. Phys. Chem. B* **1997**, *101*, 10281-10289.

(3) Schlichthörl, G.; Park, N. G.; Frank, A. J. Evaluation of the Charge-Collection Efficiency of Dye-Sensitized Nanocrystalline TiO_2 Solar Cells. *J. Phys. Chem. B* **1999**, *103*, 782-791.

(4) Schlichthörl, G.; Huang, S. Y.; Sprague, J.; Frank, A. J. Band Edge Movement and Recombination Kinetics in Dye-Sensitized Nanocrystalline TiO_2 Solar Cells: A Study by Intensity Modulated Photovoltage Spectroscopy. *J. Phys. Chem. B* **1997**, *101*, 8141-8155.
(5) Fisher, A. C.; Peter, L. M.; Ponomarev, E. A.; Walker, A. B.; Wijayantha, K. G. U. Intensity Dependence of the Back Reaction and Transport of Electrons in Dye-Sensitized Nanacrystalline TiO_2 Solar Cells. *J. Phys. Chem. B* **2000**, *104*, 949-958.
(6) Fabregat-Santiago, F.; Garcia-Belmonte, G.; Bisquert, J.; Zaban, A.; Salvador, P. Decoupling of Transport, Charge Storage, and Interfacial Charge Transfer in the Nanocrystalline TiO_2/Electrolyte System by Impedance Methods. *J. Phys. Chem. B* **2002**, *106*, 334-339.
(7) Peter, L. M. Characterization and Modeling of Dye-Sensitized Solar Cells. *J. Phys. Chem. C* **2007**, *111*, 6601-6612.
(8) van de Lagemaat, J.; Kopidakis, N.; Neale, N. R.; Frank, A. J. Effect of Nonideal Statistics on Electron Diffusion in Sensitized Nanocrystalline TiO_2. *Phys. Rev. B* **2005**, *71*, 035304.
(9) Zhu, K.; Kopidakis, N.; Neale, N. R.; van de Lagemaat, J.; Frank, A. J. Influence of Surface Area on Charge Transport and Recombination in Dye-Sensitized TiO_2 Solar Cells. *J. Phys. Chem. B* **2006**, *110*, 25174-25180.
(10) Bisquert, J.; Vikhrenko, V. S. Interpretation of the Time Constants Measured by Kinetic Techniques in Nanostructured Semiconductor Electrodes and Dye-Sensitized Solar Cells. *J. Phys. Chem. B* **2004**, *108*, 2313-2322.
(11) Cao, F.; Oskam, G.; Meyer, G. J.; Searson, P. C. Electron Transport in Porous Nanocrystalline TiO_2 Photoelectrochemical Cells. *Journal of Physical Chemistry* **1996**, *100*, 17021-17027.
(12) de Jongh, P. E.; Vanmaekelbergh, D. Trap-Limited Electronic Transport in Assemblies of Nanometer-Size Tio2 Particles. *Physical Review Letters* **1996**, *77*, 3427-3430.
(13) Nelson, J.; Haque, S. A.; Klug, D. R.; Durrant, J. R. Trap-Limited Recombination in Dye-Sensitized Nanocrystalline Metal Oxide Electrodes. *Phys. Rev. B* **2001**, *63*, 205321.
(14) Solbrand, A.; Lindstrom, H.; Rensmo, H.; Hagfeldt, A.; Lindquist, S. E.; Sodergren, S. Electron Transport in the Nanostructured TiO_2-Electrolyte System Studied with Time-Resolved Photocurrents. *J. Phys. Chem. B* **1997**, *101*, 2514-2518.
(15) van de Lagemaat, J.; Frank, A. J. Nonthermalized Electron Transport in Dye-Sensitized Nanocrystalline TiO_2 Films: Transient Photocurrent and Random-Walk Modeling Studies. *J. Phys. Chem. B* **2001**, *105*, 11194-11205.
(16) Boschloo, G.; Hagfeldt, A. Activation Energy of Electron Transport in Dye-Sensitized TiO_2 Solar Cells. *J. Phys. Chem. B* **2005**, *109*, 12093-12098.
(17) Kopidakis, N.; Benkstein, K. D.; van de Lagemaat, J.; Frank, A. J. Transport-Limited Recombination of Photocarriers in Dye-Sensitized Nanocrystalline TiO_2 Solar Cells. *J. Phys. Chem. B* **2003**, *107*, 11307-11315.
(18) Villanueva, J.; Anta, J. A.; Guillen, E.; Oskam, G. Numerical Simulation of the Current-Voltage Curve in Dye-Sensitized Solar Cells. *J. Phys. Chem. C* **2009**, *113*, 19722-19731.
(19) Peter, L. M.; Duffy, N. W.; Wang, R. L.; Wijayantha, K. G. U. Transport and Interfacial Transfer of Electrons in Dye-Sensitized Nanocrystalline Solar Cells. *J. Electroanal. Chem.* **2002**, *524*, 127-136.